Exceptionally Stiff Two-Dimensional Molecular Crystal by Substrate-Confinement

Jun Zhang,[†] Bingkai Yuan,[†] Pengcheng Chen,[†] Zhihai Cheng,[*,†] Wei Ji,[*,‡] and Xiaohui Qiu[*,†]

[†]CAS Key Laboratory of Standardization and Measurement for Nanotechnology, National Center for Nanoscience and Technology, Beijing 100190, China and
[‡]Department of Physics and Beijing Key Laboratory of Optoelectronic Functional Materials & Micro-nano Devices, Renmin University of China, Beijing 100872, China

ABSTRACT We demonstrated an approach to effectively apply in-plane pressures to molecular layers by utilizing the substrate confinement effect. The compressed crystal structure and mechanical behaviors of carbon monoxide (CO) monolayer subjected to the confinement of Cu(100) substrate were jointly investigated by low temperature scanning tunneling microscopy experiments and first-principles density functional theory calculations. By increasing molecular coverage, an exceptionally large Young's modulus of 33 GPa was derived for the constrained CO monolayer film. This extreme in-plane pressure leads to site-specific tilting geometries, polymeric-like electronic states, and vibrational behaviors of CO molecules in the compressed phases. These results provide an extended understanding of the physical and chemical properties of intermolecular interactions in this fundamental system.

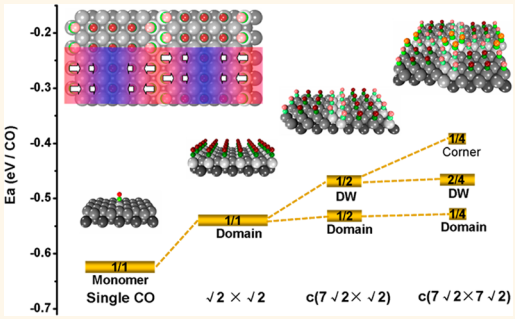

KEYWORDS: carbon monoxide · Cu(100) · Young's modulus · Pauli repulsion · substrate-confinement

External pressure has a significant effect on the physical and chemical properties of materials.[1−3] When the size of materials goes down to the nanoscale, however, it remains a challenge to apply external pressures to nanomaterials due to technical difficulties in experimental setup. Pioneering studies had demonstrated that scanning probe based cantilever technique can apply tunable shear stress on low-dimensional covalent materials, such as carbon nanotube,[4−6] and graphene layers.[7−9] External in-plane (uniaxial) stress is of more importance than shear stress in terms of tuning physical properties of one (two)-dimensional (1(2)D) materials since it directly changes the in-plane interatomic distances of materials. The cantilever technique is helpless in providing in-plane stress which was successfully achieved by employing the lattice mismatch between two materials at the interface of heteroepitaxial thin films. The mismatch leads to an interface stress, which effectively applies a 2D pressure to the epitaxial film, giving rise to, *e.g.*, induced superconductivity in FeSe and extremely high magnetic field in graphene.[10−12] In these interfaces, the effective pressure applied, however, cannot to be continuously tuned.

The continuously tunable effective pressure allows to investigate the evolution of, *e.g.*, mechanical, properties of low-dimensional materials. However, only few studies were reported in molecular crystals.[13,14] In two previous demonstrations, 2D molecular crystals were formed on coinage metal surfaces and the in-plane pressure was realized by changing the intermolecular distances governed by surface coverage.[13,14] A Young's modulus of approximately 1 GPa was revealed by a parabolic fitting of stress as a function of strain. They are rather soft even for molecular crystals, which limits the range of the applicable effective pressure. An interesting question thus arises that whether it is possible to build a "harder" 2D molecular crystal, so that s wider range of in-plane pressure can be applied, which may give rise to new physical or chemical phenomena in the molecular crystal.

The harder the crystal, the stronger the intermolecular repulsion. In the early examples, the repulsion, stemmed from side chain and outer H atoms,[13,14] was in the form of van der Waals (vdW). To realize harder 2D crystals,

* Address correspondence to chengzh@nanoctr.cn, wji@ruc.edu.cn, xhqiu@nanoctr.cn.

Received for review August 11, 2014 and accepted October 27, 2014.

Published online October 27, 2014
10.1021/nn505969v

the repulsion must be stronger than vdW. Carbon monoxide, being employed to functionalize tips for imaging the Pauli repulsion force, was believed to have strong intermolecular repulsion, which may fit the requirement of strong repulsion. The CO/Cu(100) monolayer crystal also has various phases with respect to coverage, *e.g.*, the $\sqrt{2} \times \sqrt{2}$ normal phase (NP) and more compact phases, namely, the "compressed phases" (CPs) of, *i.e.*, $c(7\sqrt{2} \times \sqrt{2})$ (CP7) and $c(5\sqrt{2} \times \sqrt{2})$ (CP5, in doubt, not observed in real space),[15,16] which might thus be an ideal prototype system for investigating the evolution of structural, mechanical, and electronic properties in a harder 2D molecular crystal.

In this paper, using a low temperature scanning tunneling microscope (STM), we report a discovery of 2D CPs, *i.e.*, phases $c(9\sqrt{2} \times 9\sqrt{2})$ (CP9-9), $c(9\sqrt{2} \times 7\sqrt{2})$ (CP9-7),, and $c(7\sqrt{2} \times 7\sqrt{2})$ (CP7-7), which are denser than the previously known "most" dense CP7 or CP5;[16] while sparse CPs of CP11 and CP9 were also observed as well as the confirmed CP5 phase. The discovery completes the evolution of process of Cu/Cu(100) from normal phase to 1D striped and then to 2D network compressed phases, which allows to derive the stiffness of the crystal. In line with density functional theory (DFT) calculations based on a continuum elastic model, the 2D crystal was predicted a Young's modulus of 33 GPa, exceptionally larger than usual molecular crystals of roughly 10 GPa. Such a high stiffness, as suggested by DFT, comes from the intermolecular Pauli repulsion. The Cu−CO attraction overcomes this repulsion forming CO molecules into a 2D crystal. We call the Cu−CO attraction "surface confinement". A certain in-plane pressure is thus induced by the substrate confinement, which is tunable by adjusting the coverage of CO molecules on Cu(100). Additionally, it was found that the CO molecules at the domain walls (DW) (in 1D) and chiral interactions (CI) (in 2D) have specific tilting configurations, which shows different local electronic density of states and vibrational behaviors from the normal $\sqrt{2} \times \sqrt{2}$ domains (ND), and most likely, gives rise to the formation of polymeric-like electronic states in the CO monolayer.

RESULTS AND DISCUSSION

Figure 1 illustrates the structural evolution of the CO/Cu(100) monolayer. The previously reported NP,[17] as shown in Figure 1a inset, was observed during the *in situ* deposition process when the CO coverage reached 0.5 ML, which indicated a rather high mobility of CO on Cu(100) at the liquid nitrogen temperature. Compressed phases appear when additional molecules were dosed onto the normal phase. At the early stage, locally ordered structures of CPs were found, *i.e.*, the CP11 and CP9. The interdomain wall distances of these two CPs are and $5.5\sqrt{2}a$ and $4.5\sqrt{2}a$, respectively, where a = 2.55 Å is the nearest surface

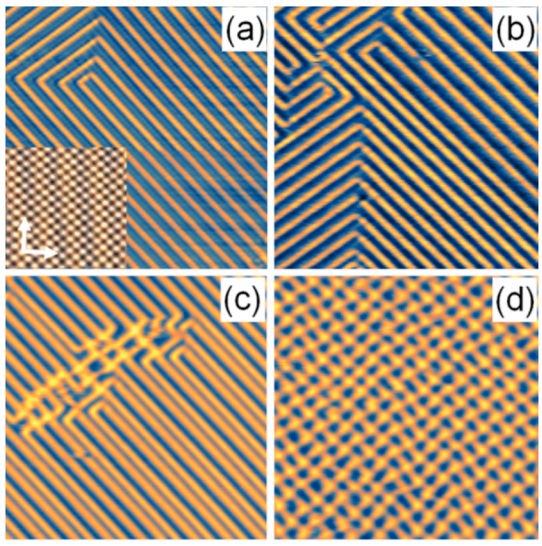

Figure 1. STM images of CO/Cu(100) in phases of NP (a) inset, CP7 (a), a mixture of CP7 and CP5 (b), a mixture of 1D and 2D (c), and 2D network (d). The scan area is 20 nm × 20 nm. The arrows in the (a) inset indicates the ⟨110⟩ directions of Cu(100). The rows (bright lines in the images) correspond to the DWs growing along the ⟨100⟩ directions, which end only at Cu step edges.

Cu−Cu distance. The distance shortened when more CO molecules were dosed, eventually forming a denser CP7 phase at the coverage of θ = 4/7 ≈ 0.57 ML, as shown in Figure 1a, consistent with the previous results.[16] Although CP7 was previously reported as the "densest" phase, an even denser phase of CP5 was obtained in our experiment, as shown in Figure 1b. All of these CPs are "1D-like" that DWs in them do not cross each other although orthogonal turnings were often observable. These 1D CPs evolves into crossed DWs when further increasing the coverage, as shown in Figure 1c,d, as well as the movie available in the associated Supporting Information.[18] These 2D CPs have never been reported before. A careful analysis of the interdomain wall distances indicates that the 2D CP is a mixture of the CP9-9, CP9-7 and CP7-7 superstructures, in which the normal $\sqrt{2} \times \sqrt{2}$ domains (NDs) were surrounded by the crossed DWs running along the ⟨100⟩ directions. Further deposition did not give rise to denser CPs, *e.g.*, CP3, CP7-5 or CP5-5.

DFT calculations were employed to reveal the structural details of these CPs. Figure 2 shows the fully relaxed atomistic structures of phases CP9, CP7, CP5 and CP7-7, and their corresponding STM images. These bright dots in the STM images represent the position of the oxygen atoms.[19] The side views of molecular configuration show that CO molecules are strongly tilted outward at the DWs, while the C−Cu bond lengths are kept unchanged. Table 1 summarizes the detail values of the tilting angle and bond lengths. The CO molecules next to the DW COs are also tilted in CP9 and CP7 and the C−Cu bond lengths of these molecules are the same to those of the COs in NP.

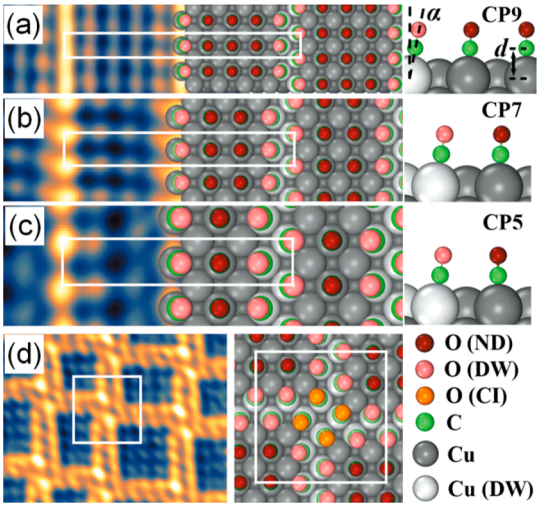

Figure 2. Molecular resolution STM images of CP9 (a), CP7 (b), CP5 (c), and a mixture of CP9-9, CP9-7, and CP7-7 (d) and their corresponding theoretical models in top- and side-views. Solid-white rectangles in (a−c) indicate the lattice of the conventional cells, and the square in (d) highlights the chiral intersection (CI). Angle α is the molecular tilting angle and *d* is the C−Cu distance.

TABLE 1. Structural Details of CO/Cu(100) Normal and Compressed Phases

	C−O (Å)			Cu−C (Å)			
structure	ND	DW	CI	ND	DW	CI	α (deg)
CP9	1.161	1.162	-	1.873	1.876	-	10.1
CP7	1.161	1.162	-	1.872	1.876	-	10.0
CP5	1.160	1.161	-	1.872	1.876	-	8.9
CP3	-	1.161	-	-	1.876	-	-
CP7-7	1.161	1.163	1.163	1.864	1.871	1.874	-
CP5-5	-	1.162	1.163	-	1.867	1.872	-
CP3-3	-	-	1.161	-	-	1.877	-
CO (g)	1.148/1.13 (Exp)			-			-
Single CO (s)	1.163			1.860			-

Figure 2d shows the theoretical model of the CP7-7 phase that contains a CI comprising orthogonally kinked DWs and an associated molecule-resolved STM image where CP9-9, CP9-7, and CP7-7 were identified. Unlike that in 1D CPs, the NDs are surrounded by orthogonally crossed DWs in 2D CPs. The difference of C−Cu bond lengths from those of 1D CPs is within 0.003 Å for both NDs and DWs, and the C−O bond length at CIs is 0.01 Å longer than that in NDs. All of the tilting angles, however, are up to 2° larger than the corresponding angles in less dense 1D CPs, which essentially does not change the thickness of the adlayer.

Adsorption energy of CO molecules was calculated for all considered CPs. Two categories of adsorption energies were presented in Figure 3, *i.e.*, the energy gains per molecule (E_{ads-M}) and per surface Cu atom (E_{ads-S}) upon the adsorption. The former one reflects the strength of molecule−substrate and intermolecular interactions, and the latter one represents the stability of the molecule-covered surface. The absolute value of E_{ads-M} decreases with respect to the increase of coverage, which indicates that the E_{ads-M} at DWs is smaller than that in NDs. Negative values of E_{ads-M} suggest that the formation of every considered CP is energetically favorable. Some structures, however, were not observed in the experiment. It could be explained by Figure 3b, where the evolution of E_{ads-S} with the increasing coverage was plotted. The 1D E_{ads-S} (in blue) continuously drops before the coverage (θ) reaches 0.6. At a higher coverage of 0.64, CP7-7 keeps the trend of dropping, although the *E* goes higher in CP3 (θ = 0.67). Denser phases of CP5-5 and CP3-3, similar to CP3, fleetly lose their stability that E quickly goes smaller. A turning point of E_{ads-S} was thus found at CP7-7, which means the formation of superstructures with a higher coverage than CP7-7 is energetically unfavorable, unlikely being observed in our experiments.

We consider these appeared CPs as a quasi-continuous evolution of the CO/Cu(100) adalyer to reveal the underlying correlations among them. The continuous reduced E with increasing coverage implies repulsive interactions among these CO molecules under the substrate-confinement pressure. The response to the pressure is commonly evaluated by plotting strain energy density *U* as a function of strain ε. The actual strain energy density *U* can be calculated by $U(i,0) = (E_{ads-M-i} - E_{ads-M-0})\theta_i/(S_0 h_0)$, where $E_{ads-M-i}$ and $E_{ads-M-0}$ denote the averaged E_{ads-M} of CO in different CPs and the noncompressed NP, respectively, S_0, the area occupied by one Cu atom on Cu(100) surface, is 6.5 Å^2, and h_0, the averaged adlayer thickness, is the total length of Cu−C and C−O bonds, approximately 3 Å. The strain ε can be determined by $\varepsilon(i,0) = [(1/\theta_i)^{1/2} - (1/\theta_0]^{1/2})/(1/\theta_0)^{1/2}$, where θ_0 and θ_i denote the coverage of the ND and different CPs, respectively.

Figure 3c plots the $U(\varepsilon)$ of the CO adlayer, showing a Hookean response characterized by the strain energy density *U* increasing quadratically with the strain ε. For this particular case that the CO adlayer is in-plane compressed by chemical attractions, *U* simplifies to $U = E\varepsilon^2$, where *E* is the Young's modulus. A quadratic fit of the data set of Figure 3c yields the Young's modulus of the CO adlayer of approximately 33 GPa, which is substantially larger than that of molecular solids (typically range between 2 to 15 GPa, *e.g.*, 12.4 GPa for CO2-I), but lower than that of solid copper (∼124 GPa). The Young's modulus of the CO layer has a theoretical upper limit that cannot exceed the Young's modulus of the Cu(100) substrate which was employed as an external constrain to the CO layer.

The Young's modulus generally correlates with the bond stiffness of materials by $E = S/a_0$, where *S* and a_0 are the bond stiffness and the equilibrium intermolecular distance. The equilibrium intermolecular distance

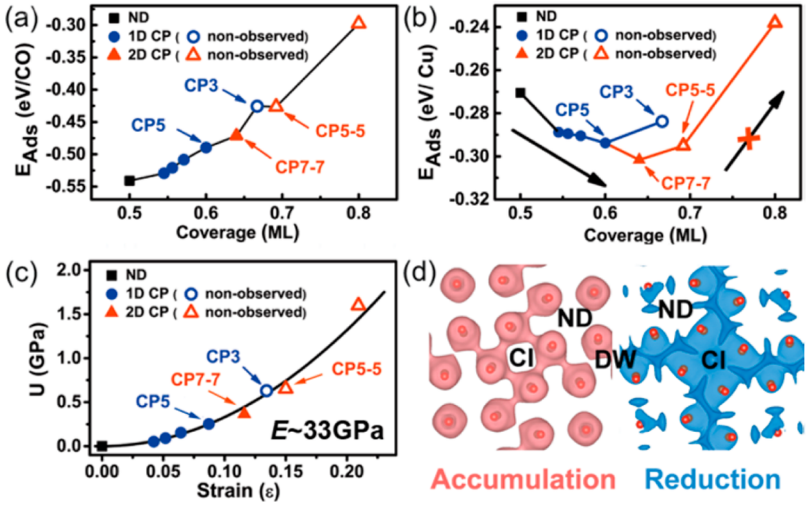

Figure 3. Energetic evolution of the CO/Cu(100) adlayer with the increasing coverage (a−c). Adsorption energies per molecule (a) and per surface Cu (b) as functions of coverage. (c) Strain energy density as a function of the compressive strain. The quadratic fit yields a Young's modulus of ~33 GPa. (d) Top-views (isosurface is 0.002e/Å^2) of the differential charge density by subtracting individual CO molecules from a constrained CO adlayer in configuration CP7-7. Light-red and blue colors represent charge reduction and accumulation.

a_0 of COs is ~3.65 Å for CO/Cu(100), which leads to an equivalent bond stiffness of ~11.8 N/m. This value is smaller than that of typical metallic (15−75 N/m) and covalent (50−180 N/m) bonds, but comparable with the typical value of ionic bonds (8−24 N/m) and much larger than that of van der Waals force (0.5−1 N/m). Intermolecular interactions of polarized molecules on surfaces were usually supposed to be repulsive due to electric dipole−dipole interactions.[20,21] Such a high stiffness of ~11.8 N/m, however, cannot be ascribed to the relatively weak vdW-like long-range dipole−dipole interactions. A similar strong repulsive force-constant of ~10.5 ± 1.5 N/m had been experimentally estimated for the CO on Pd(110) system, while have been ascribed to the steric Pauli repulsion between the nearest neighbor molecules.[22−24] The plot of differential charge density explicitly shows electron density accumulations around COs, as shown in Figure 3d left, where pipelines of electron density were found at CIs and DWs. These charges, as shown Figure 3d right, stem from the electron density reductions at the interstitial region of the CO molecules, which results in dominative Pauli repulsion between the nearest COs. The Pauli-repulsion force can be partially relaxed by tilting and/or bending the DW (CI) molecules, making a nonterminal adsorption site.[16]

Tilting and bending CO molecules do occur at the DWs and CIs, as shown in Figure 2, owing to efficiently reducing of Pauli repulsion among CO molecules.[16] These local structural relaxations may significantly vary the site-specific adsorption energy, local electronic structures, and other properties of the CO adlayer. The site-specific adsorption energies of CO molecules in the ND and all CPs were summarized in the associated Supporting Information.[22] The adsorption energy of CO (E_{ads-M}) in NP is −541 meV, 85 meV smaller than that of an isolated CO molecule on Cu(100) of −626 meV, indicating repulsive dipole−dipole intermolecular interactions in NDs.[29] By fitting the E of a series of CPs, it was found that the adsorption energy of a CO in ND is −569 ± 5 and −448 ± 4 meV for that at DW. Given the both values, the adsorption energy at CI was derived as −420 ± 9 meV for the denser phase of CP7-7. These four adsorption energies of the NP and CPs can be grouped into two categories, one for the ND in the range from −569 to −541 meV and the other for the DW and CI in the range from −448 to −420 meV. These results explain the two different desorption temperatures of 180 and 135 K observed experimentally,[26] in which the assessment of the 135 K value was previously uncertain.

The ND and DW yield distinctly different properties in terms of local electronic structures. Phase CP5 is the simplest phase containing both ND and DW, which is preferred in our analysis of electronic structures. The local densities of states (LDOS) of a ND and DW carbon atom in CP5, shown in Figure 4, are superposed. Either of them has at least one peak that the other does not have, which indicates that certain electronic states of CO molecules are spatial-separately distributed. Two states, *i.e.*, S-DW and S-ND, illustrated as two peaks in Figure 4, were chosen for further discussion, while the rest states essentially share the same physics with the specified two. States S-DW and S-ND reside at 0.55 and 0.62 eV above the Fermi energy, respectively. According to the plots of charge density (Figure 4 inset), state S-DW is strictly confined in the DW region while state S-ND has very small populations on CO molecules in the DW region. The white holes in the charge density plots, as indicated by the black and red rings, represent pipelines of charge density between CO molecules along the direction perpendicular to the

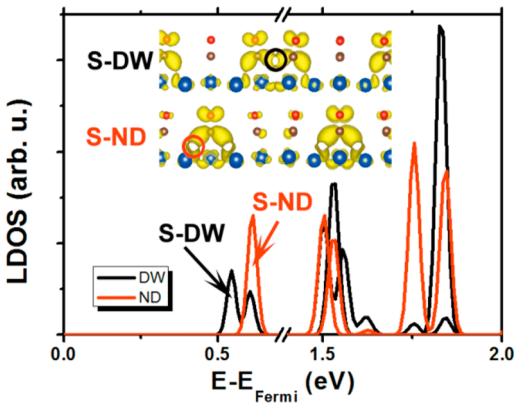

Figure 4. Projected local density of states for C atoms at DW (black) and in ND (red), which explicitly illustrates the spatial splitting of the thin film into two regions in terms of electron structures. Other states shown in the LDOS yield similar features or have comparable populations at both DW and ND. The charge densities of states S-DW and S-ND residing at 0.55 and 0.62 eV were plotted as inset.

figure, indicating intermolecular electronic hybridization. Such hybridization, different from substrate-mediated and superatom-orbital-interaction ones,[27,28] may provide site- and orientation-specified electron conducting channels in molecular adlayers.

The vibrational behaviors of adsorbates play important roles in a wide range of surface physical and chemical process. We further discuss the site-specific vibration frequencies of CO molecules in CP7−7, the densest phase in our experiments. The four fundamental vibrational modes of CO on Cu(111) in the $\sqrt{2} \times \sqrt{2}$ phase had been experimentally identified by infrared reflection-adsroption spectroscopy (IRAS) and helium atom scattering.[29] The C−O (ν_1) and C−Cu (ν_2) stretching modes indicate the vertical interaction strength of C−O and C−Cu bonds, while the frustrated rotation (ν_3) and translation (ν_4) modes represent the lateral interaction.

Here, we compare these four vibrational frequencies of CO molecules at CI, DW and ND to identify their site-specific local environment and properties (Table 2). The detailed Reflection Adsorption Infrared spectroscopy (RAIRS) study by J. C. Cook *et al.* indicated an evolution of frequency (or energy), width, and peak intensity of the C−O stretch vibration (ν_1) with the increasing of CO coverage.[30] A clear narrowing occurs initially as the coverage increase to 0.5 ML (the homogeneous ordered $\sqrt{2} \times \sqrt{2}$ phase), and then the peak broadens again. This is clearly due to the site-specific adsorption behavior of COs in the inhomogeneous compressed phases observed and discussed in our

TABLE 2. Vibrational Behaviors of CO/Cu(100) in the Compressed Phase of CP7-7

structures	CP7-7			
sites	CI	DW	ND	NP (exp)[33]
C−O stretching (ν_1, cm^{-1})	1975.21	1975.74	1988.45	2086
Cu−C stretching (ν_2, cm^{-1})	310.20	308.14	312.82	345
Frustrated rotation (ν_3, cm^{-1})	283.65 299.54	279.71 289.85	274.03 276.38	285
Frustrated translation (ν_4, cm^{-1})	86.21 105.09	80.75 87.08	80.70 85.00	32

work. Generally, the C−O stretching of CO decreased from at ND to DW and CI. It is striking that the C−O stretching is almost same at CI and DW, while the Cu−C stretching at CI is even larger than that at DW site. This could be due to the Cu atoms underneath the CO at CI being 0.02 Å higher than other normal substrate Cu atoms. The frustrated modes are degenerated in the normal $\sqrt{2} \times \sqrt{2}$ phase, while split into two submodes in the compressed $7\sqrt{2} \times 7\sqrt{2}$ phase due to the directional repulsions. Both the frustration modes and the separation between the two submodes of CO significantly increased from at ND to DW and CI. These site-specific vibrational behaviors of COs in the compressed phases play important roles in determining the physical and chemical properties of this fundamental adsorption system.

CONCLUSIONS

In summary, the coverage-dependent evolutions of CO monolayer films were investigated by STM experiments and DFT calculations. We demonstrated that an exceptionally large Young's modulus of 33 GPa was achieved in the monolayers, ascribed to the introduction of substrate confinement. The substrate-molecule interactions, constraining CO monolayer, provide an equivalent external pressure of up to 0.25 GPa (in CP5) and 0.37 GPa (in CP7-7) as derived by DFT calculations. Local electronic structures and vibrational behaviors of the CO layer are not homogeneous at the domain walls and chiral intersections. Intermolecular wave function overlap was found in certain electronic states, which suggests the formation of electron conducting channels in the CO layer led by substrate-confinement-induced pressure. These results manifest a feasible method to introducing in-plane pressure to molecular (mono)-layers, enabling to tailor the mechanical and electronic properties of molecular layers.

METHODS

The experiments were performed with an Omicron UHV low temperature STM system at a base pressure below 10^{-10} mbar. The Cu(100) single crystal (MaTeck) was cleaned by repeated cycles of Neon ion sputtering and annealing at ~850 K. CO was *in situ* deposited onto the Cu(100) surface kept at liquid

nitrogen (LN_2) temperature. The coverage of CO molecules on the surface was controlled by adjusting the dosing time. The images were acquired at LN_2 temperature and with a cut Pt/Ir tip. The bias voltages referred to in STM images are the sample voltages.

Calculations were carried out by the general gradient approximation in the form of RPBEfor the exchange-correlation potential,[31] the projector augmented wave method,[32] and a plane wave basis set as implemented in the Vienna *ab initio* simulation package.[33,34] The energy cutoff for plane-wave basis was set to 650 eV. Six layers of Cu atoms, separated by a 20-Å vacuum region, were employed to model the Cu surfaces. The molecule was only put on one side of the slab with a dipole correction. A $10 \times 10 \times 1$ k-mesh was used to sample the 2D Brillouin Zone of a $\sqrt{2} \times \sqrt{2}$ supercell, while the density of k-meshes keeps for other supercells. Three times denser k-sampling was applied to both surface directions in adsorption energy calculations. In geometry optimization, all atoms except those for the bottom three layers were fully relaxed until the residual force per atom was less than 0.005 eV/Å. All these parameters ensure the convergence of adsorption energy in 1 meV per molecule. The vibrational frequencies of CO at normal domain (ND), domain wall (DW) and chiral intersections (CI) were evaluated in a $7\sqrt{2} \times 7\sqrt{2}$ supercell by the frozen phonon method. Each dynamic matrix for calculating vibrational frequencies was constructed by moving the atoms of a CO molecule. It is much heavier of a Cu atom than a C or O atom, so that the vibrational properties shall not be qualitatively affected by the exclusion of Cu atom in constructing the dynamic matrix.

Conflict of Interest: The authors declare no competing financial interest.

Acknowledgment. This project is partially supported by the Ministry of Science and Technology (MOST) of China (Grant Nos. 2012CB933001, 2012CB932704), the Natural Science Foundation of China (NSFC) (Grant Nos. 21173058, 21203038, 11004244, 11274380), the Beijing Natural Science Foundation (BNSF) (Grant No. 2112019), and the Basic Research Funds in Renmin University of China from the Central Government (Grant No. 12XNLJ03), Supercomputing Center, CNIC, CAS. W. Ji was supported by the Program for New Century Excellent Talents in University. Calculations were performed at the Physics Lab for High-Performance Computing (PLHPC) of Renmin University of China and Shanghai Super-computing Center.

Supporting Information Available: Movie of selected frames from a series of STM images during *in situ* CO deposition (avi), tables listing the structures and the corresponding DFT calculated energy of different CO phases and site-specific adsorption energies of CO molecules for a series of adsorption phases on Cu(100). This material is available free of charge *via* the Internet at http://pubs.acs.org.

REFERENCES AND NOTES

1. Hemley, R. J. Effects of High Pressure on Molecules. *Annu. Rev. Phys. Chem.* **2000**, *51*, 763–800.
2. Schettino, V.; Bini, R. Molecules under Extreme Conditions: Chemical Reactions at High Pressure. *Phys. Chem. Chem. Phys.* **2003**, *5*, 1951–1965.
3. Sun, J.; Klug, D. D.; Pickard, C. J.; Needs, R. J. Controlling the Bonding and Band Gaps of Solid Carbon Monoxide with Pressure. *Phys. Rev. Lett.* **2011**, *106*, 145502.
4. Yu, M.-F.; Lourie, O.; Dyer, M. J.; Moloni, K.; Kelly, T. F.; Ruoff, R. S. Strength and Breaking Mechanism of Multiwalled Carbon Nanotubes under Tensile Load. *Science* **2000**, *287*, 637–640.
5. Yu, M.-F.; Files, B. S.; Arepalli, S.; Ruoff, R. S. Tensile Loading of Ropes of Single Wall Carbon Nanotubes and their Mechanical Properties. *Phys. Rev. Lett.* **2000**, *84*, 5552–5555.
6. Salvetat, J.-P.; Bonard, J.-M.; Thomson, N.; Kulik, A.; Forro, L.; Benoit, W.; Zuppiroli, L. Mechanical Properties of Carbon Nanotubes. *Appl. Phys. A: Mater. Sci. Process.* **1999**, *69*, 255–260.
7. Lee, C.; Wei, X.; Kysar, J. W.; Hone, J. Measurement of the Elastic Properties and Intrinsic Strength of Monolayer Graphene. *Science* **2008**, *321*, 385–388.
8. Smolyanitsky, A.; Killgore, J. P.; Tewary, V. K. Effect of Elastic Deformation on Frictional Properties of Few-Layer Graphene. *Phys. Rev. B* **2012**, *85*, 035412.
9. Lee, C.; Wei, X.; Li, Q.; Carpick, R.; Kysar, J. W.; Hone, J. Elastic and Frictional Properties of Graphene. *Physi. Status Solidi B* **2009**, *246*, 2562–2567.
10. Song, C.-L.; Wang, Y.-L.; Jiang, Y.-P.; Wang, L.; He, K.; Chen, X.; Hoffman, J. E.; Ma, X.-C.; Xue, Q.-K. Suppression of Superconductivity by Twin Boundaries in FeSe. *Phys. Rev. Lett.* **2012**, *109*, 137004.
11. Wang, Q.-Y.; Li, Z.; Zhang, W.-H.; Zhang, Z.-C.; Zhang, J.-S.; Li, W.; Ding, H.; Ou, Y.-B.; Deng, P.; Chang, K.; *et al.* Interface-Induced High-Temperature Superconductivity in Single Unit-Cell FeSe Films on $SrTiO_3$. *Chin. Phys. Lett.* **2012**, *29*, 037402.
12. Levy, N.; Burke, S. A.; Meaker, K. L.; Panlasigui, M.; Zettl, A.; Guinea, F.; Neto, A. H. C.; Crommie, M. F. Strain-Induced Pseudo-Magnetic fields Greater than 300 T in Graphene Nanobubbles. *Science* **2010**, *329*, 544–547.
13. Sun, D.; Kim, D.-H.; Le, D.; Borck, O.; Berland, K.; Kim, K.; Lu, W.; Zhu, Y.; Luo, M.; Wyrick, J.; *et al.* Effective Elastic Properties of a van der Waals Molecular Monolayer at a Metal Surface. *Phys. Rev. B* **2010**, *82*, 201410.
14. Cun, H.; Wang, Y.; Du, S.; Zhang, L.; Zhang, L.; Yang, B.; He, X.; Wang, Y.; Zhu, X.; Yuan, Q.; *et al.* Tuning Structural and Mechanical Properties of Two-Dimensional Molecular Crystals: The Roles of Carbon Side Chains. *Nano Lett.* **2012**, *12*, 1229–1234.
15. Hermse, C. G. M.; Jansen, M. M. M.; van Bavel, A. P.; Lukkien, J. J.; van Santen, R. A.; Jansen, A. P. J. On the Nature of Dense CO Adlayers on fcc(100) Surfaces: A Kinetic Monte Carlo Study. *Phys. Chem. Chem. Phys.* **2010**, *12*, 461–473.
16. Thamankar, R.; Meyerheim, H. L.; Ernst, A.; Ostanin, S.; Maznichenko, I. V.; Soyka, E.; Mertig, I.; Kirschner, J. Tilting, Bending, and Nonterminal Sites in CO/Cu(001). *Phys. Rev. Lett.* **2011**, *106*, 106101.
17. Biberian, J.; Hove, M. V. A New Model for CO Ordering at High Coverages on Low Index Metal Surfaces: A Correlation between LEED, HREELS and IRS. I. CO Adsorbed on fcc (100) Surfaces. *Surf. Sci.* **1982**, *118*, 443–464.
18. Supporting Information is available online.
19. Feng, M.; Cabrera-Sanfelix, P.; Lin, C.; Arnau, A.; Sanchez-Portal, D.; Zhao, J.; Echenique, P. M.; Petek, H. Orthogonal Interactions of CO Molecules on a One-Dimensional Substrate. *ACS Nano* **2011**, *5*, 8877–8883.
20. Blyholder, G. Molecular Orbital View of Chemisorbed Carbon Monoxide. *J. Phys. Chem.* **1964**, *68*, 2772–2777.
21. Ahner, J.; Mocuta, D.; Ramsier, R. D.; Yates, J. T., Jr. Kinetics Measurements of CO Photooxidation on Pt(111). *J. Chem. Phys.* **1996**, *105*, 6553–6559.
22. Kato, H.; Kawai, M.; Yoshinobu, J. Switching in the Molecular Orientation Ruled by Steric Repulsion of Adsorbed CO on Pd(110). *Phys. Rev. Lett.* **1999**, *82*, 1899–1902.
23. Kato, H.; Okuyama, H.; Ichihara, S.; Kawai, M.; Yoshinobu, J. Lateral Interactions of CO in the (2×1)p2mg structure on Pd(110): Force Constants between tilted CO molecules. *J. Chem. Phys.* **2000**, *112*, 1925–1936.
24. Lang, N. D.; Holloway, S.; Nørskov, J. K. Electrostatic Adsorbate-Adsorbate interactions: The poisoning and Promotion of the Molecular Adsorption Reaction. *Surf. Sci.* **1985**, *150*, 24–38.
25. Persson, B. N. J.; Ryberg, R. Vibrational Interaction between Molecules Adsorbed on a Metal Surface: The Dipole–Dipole Interaction. *Phys. Rev. B* **1981**, *24*, 6954–6970.
26. Liu, C.; Tobin, R. G. Bonding-Site Dependence of Surface Resistivity: CO on Epitaxial Cu(100) Films. *J. Chem. Phys.* **2007**, *126*, 124705.
27. Ji, W.; Lu, Z.-Y.; Gao, H.-J. Multichannel Interaction Mechanism in a Molecule-Metal Interface. *Phys. Rev. B* **2008**, *77*, 113406.
28. Dougherty, D. B.; Feng, M.; Petek, H.; Yates, J. T., Jr.; Zhao, J. Band Formation in a Molecular Quantum Well *via* 2D

Superatom Orbital Interactions. *Phys. Rev. Lett.* **2012**, *109*, 266802.
29. Germer, T. A.; Stephenson, J. C.; Heiweil, E. J.; Cavamagh, R. R. Hot Carrier Excitation of Adlayers: Time-Resolved Measurement of Adsorbate-Lattice Coupling. *Phys. Rev. Lett.* **1993**, *71*, 3327–3330.
30. Cook, J. C.; Clowes, S. K.; McCash, E. M. Reflection Adsorption IR Studies of Vibrational Energy Transfer Processes and Adsorption Energetics. *J. Chem. Soc., Faraday Trans.* **1997**, *93*, 2315–2322.
31. Hammer, B.; Hansen, L. B.; Nørskov, J. K. Improved Adsorption Energetics within Density-Functional Theory using Revised Perdew-Burke-Ernzerhof functionals. *Phys. Rev. B* **1999**, *59*, 7413–7421.
32. Kresse, G.; Joubert, D. From Ultrasoft Pseudopotentials to the Projector Augmented-Wave Method. *Phys. Rev. B* **1999**, *59*, 1758–1775.
33. Kresse, G.; Furthmuller, J. Efficient Iterative Schemes for *ab initio* Total-Energy Calculations using a Plane-Wave Basis Set. *Phys. Rev. B* **1996**, *54*, 11169–11186.
34. Kresse, G.; Furthmuller, J. Efficiency of Ab-initio Total Energy Calculations for Metals and Semiconductors using a Plane-Wave Basis Set. *Comput. Mater. Sci.* **1996**, *6*, 15–50.